C. R. Mecanique 344 (2016) 448–455

Contents lists available at ScienceDirect

Comptes Rendus Mecanique

www.sciencedirect.com

Travelling-wave solutions bifurcating from relative periodic orbits in plane Poiseuille flow

Subhandu Rawat [a], Carlo Cossu [a,*], François Rincon [b,c]

[a] Institut de mécanique des fluides de Toulouse, CNRS and Université de Toulouse, allée du professeur Camille Soula, 31400 Toulouse, France
[b] Université de Toulouse, UPS–OMP; IRAP, 31400 Toulouse, France
[c] CNRS, IRAP, 14, avenue Édouard-Belin, 31400 Toulouse, France

ARTICLE INFO

Article history:
Received 4 July 2015
Accepted 28 December 2015
Available online 19 March 2016

Keywords:
Fluid dynamics
Hydrodynamic stability
Transition to turbulence

ABSTRACT

Travelling-wave solutions are shown to bifurcate from relative periodic orbits in plane Poiseuille flow at $Re = 2000$ in a saddle-node infinite-period bifurcation. These solutions consist in self-sustaining sinuous quasi-streamwise streaks and quasi-streamwise vortices located in the bulk of the flow. The lower branch travelling-wave solutions evolve into spanwise localized states when the spanwise size L_z of the domain in which they are computed is increased. On the contrary, the upper branch of travelling-wave solutions develops multiple streaks when L_z is increased. Upper-branch travelling-wave solutions can be continued into coherent solutions to the filtered equations used in large-eddy simulations where they represent turbulent coherent large-scale motions.

1. Introduction

The dynamics of transitional and turbulent wall-bounded shear flows is the subject of continued interest because of its numerous applications, ranging from drag-reduction for transport applications to the physics of planetary boundary layers. A fruitful line of research has been to apply the dynamical systems approach to the understanding of subcritical transition in wall-bounded shear flows. In this context, the subcritical transition to turbulence has been related to the appearance of invariant solutions to the Navier–Stokes equations disconnected from the laminar basic state, and in particular of travelling-wave (TW) and relative periodic orbit (RPO) solutions. Travelling-wave solutions, representing saddles in phase space, have been found at Reynolds numbers lower than the transitional ones in Couette flow, [1], plane channel flow [2,3], and pipe flow [4,5]. Relative periodic orbit solutions have also been computed in plane Couette flow [6–8], plane channel [9], and pipe flows [10], and in the asymptotic suction boundary layer [11]. Global bifurcations of relative periodic orbits have been shown to be related to the transition to chaotic dynamics in plane Couette flow [12] and in magnetohydrodynamic Keplerian shear flows [13].

Invariant solutions are thought to be important not only to understand the subcritical transition, but also to gain understanding of the mechanisms of self-sustained turbulent motions at high Reynolds numbers. In particular, it was shown in a recent study [14] that the Nagata–Clever–Busse–Waleffe steady solution to the Navier–Stokes equations is connected to a solution to the filtered equations used in large-eddy simulations. This suggests that this coherent steady solution is related to turbulent large-scale motions, which are believed to be the dominant feature of the flow at high Reynolds numbers.

* Corresponding author.
E-mail address: carlo.cossu@imft.fr (C. Cossu).

http://dx.doi.org/10.1016/j.crme.2015.12.005

In a previous study [15], we have computed relative periodic orbit solutions to the Navier–Stokes equations in a plane channel at Reynolds numbers ranging from $Re = 2000$ to $Re = 5000$ in a domain periodic in the streamwise and spanwise directions with extension $2\pi h \times 2h \times 2.416h$, where h is the channel's half-width. These dimensions are typical of large-scale motions in fully developed turbulent flows. The computed solutions occupy the bulk of the flow, even at large Reynolds numbers, similarly to large-scale motions. Other solutions computed in the same flow at high Re do not have this feature, and are most likely relevant to the dynamics in the buffer layer [16,9].

The computed relative periodic orbit solutions [15] displayed the features of lower-branch solutions, which are relevant to the transition problem. In order to track their 'birth' through a bifurcation and to compute the related upper branch solutions (which are expected to provide features more related to the developed turbulent flow), we attempted to continue these solutions to lower Reynolds numbers, but were unable to extend the continuation much below $Re = 2000$. In an alternative attempt, we therefore also tried to continue the solutions by extending the size of the domain. The main objective of this paper is to show that the periodic solution disappears in an infinite-period saddle-node bifurcation as the box spanwise size is increased, giving birth to two branches of travelling-wave solutions. In the process, we found out that the upper branch displays the features of turbulent large-scale coherent motions and can be continued into a coherent solution to filtered large-eddy simulation equations, while the lower-branch solution evolves into a localized edge-state when the spanwise size of the box is further increased. A summary of the formulation of the problem and of the techniques used to isolate the periodic solutions in a plane channel flow is given in §2. The main results of the continuation are reported in §3, and discussed in §4.

2. Formulation of the problem and methods

The pressure-gradient-driven flow of an incompressible viscous fluid of constant density ρ and kinematic viscosity ν in a plane channel of height $2h$ is considered. The flow satisfies the Navier–Stokes equations:

$$\nabla \cdot \mathbf{u} = 0 \tag{1}$$

$$\frac{\partial \mathbf{u}}{\partial t} + \mathbf{u} \cdot \nabla \mathbf{u} = -\nabla p + \frac{1}{Re} \nabla^2 \mathbf{u} \tag{2}$$

where the Reynolds number $Re = U_0 h/\nu$ is defined with respect to the peak velocity U_0 of the usual laminar (parabolic) Poiseuille solution. Dimensionless velocities have been defined with respect to U_0, pressures with respect to ρU_0^2, lengths with respect to h and times with respect to h/U_0. The streamwise axis aligned with the pressure gradient is denoted by x, while the wall-normal and spanwise coordinates are denoted by y and z, and u, v and w are the velocity components along x, y and z, respectively. The flow is studied in the domain $[-L_x/2, L_x/2] \times [-1, 1] \times [-L_z/2, L_z/2]$. No-slip conditions are enforced in $y = \pm 1$ (walls), while periodic boundary conditions are enforced on the other boundaries.

In the final part of the study, new turbulent coherent solutions to the plane Poiseuille flow are sought by solving the dynamical equations for filtered motions routinely used in large eddy simulations [17,18]. The equations for the filtered motions are the usual ones (see, e.g., [19,20]):

$$\frac{\partial \overline{u}_i}{\partial x_i} = 0; \quad \frac{\partial \overline{u}_i}{\partial t} + \overline{u}_j \frac{\partial \overline{u}_i}{\partial x_j} = -\frac{\partial \overline{q}}{\partial x_i} + \nu \frac{\partial^2 \overline{u}_i}{\partial x_j^2} - \frac{\partial \overline{\tau}_{ij}^r}{\partial x_j} \tag{3}$$

where filtered quantities are denoted by an over-bar and $\overline{\tau}^r = \overline{\tau}^R - tr(\overline{\tau}^R)\mathbf{I}/3$, with $\overline{\tau}_{ij}^R = \overline{u_i u_j} - \overline{u}_i \overline{u}_j$ and $\overline{q} = \overline{p} + tr(\overline{\tau}^R)/3$. We use Smagorinsky's [21] subgrid model based on the eddy viscosity ν_t for the anisotropic residual stress tensor $\overline{\tau}_{ij}$: $\overline{\tau}_{ij}^r = -2\nu_t \overline{S}_{ij}$, where $\overline{S}_{ij}$ is the rate of strain tensor associated with the filtered velocity field, $\nu_t = D(C_s\overline{\Delta})^2 \overline{\mathcal{S}}$ and $\overline{\mathcal{S}} \equiv (2\overline{S}_{ij}\overline{S}_{ij})^{1/2}$, $\overline{\Delta} = (\overline{\Delta}_x \overline{\Delta}_y \overline{\Delta}_z)^{1/3}$. The Smagorinsky constant reference value is set to $C_s = 0.05$, as in [22,18], which is known to provide the best performance for *a posteriori* tests [23]. To avoid non-zero residual velocity and shear stress at the wall we use the wall (damping) function $D = 1 - e^{-(y^+/A^+)^2}$ with $A^+ = 25$.

Travelling-wave solutions are computed with a Newton-based iterative method implemented in the code `peanuts` [24,13], which includes parameter continuation, and is also used to analyze the linear stability of the converged solutions. `Peanuts` relies on repeated calls to numerical time-integrations of the Navier–Stokes or of the filtered equations to perform Newton iterations using a matrix-free iterative method. As in many of previous similar investigations (e.g., [3,15,11]), the search space of the solutions is restricted to those with mid-plane reflection symmetry $\{u, v, w\}(x, y, z) = \{u, -v, w\}(x, -y, z)$, which reduces the number of degrees of freedom and is known to improve convergence.

The Navier–Stokes simulations are performed with `channelflow`, which is based on a Fourier–Chebyshev–Fourier spatial pseudo-spectral discretization [25]. Solutions are advanced in time using a second-order Crank–Nicolson Runge–Kutta time stepping. Converged solutions were obtained with $32 \times 65 \times 32$ points in the streamwise, wall-normal, and spanwise directions and enforcing a constant volume flux during the simulation. These solutions are almost identical to those computed on a coarser grid $16 \times 41 \times 16$. The numerical results were further tested by recomputing the same periodic solutions on the same grid with the `diablo` code [26]. `diablo` was also used to perform the time-integrations of the filtered equations (LES) as in previous related investigations [17,18,14].

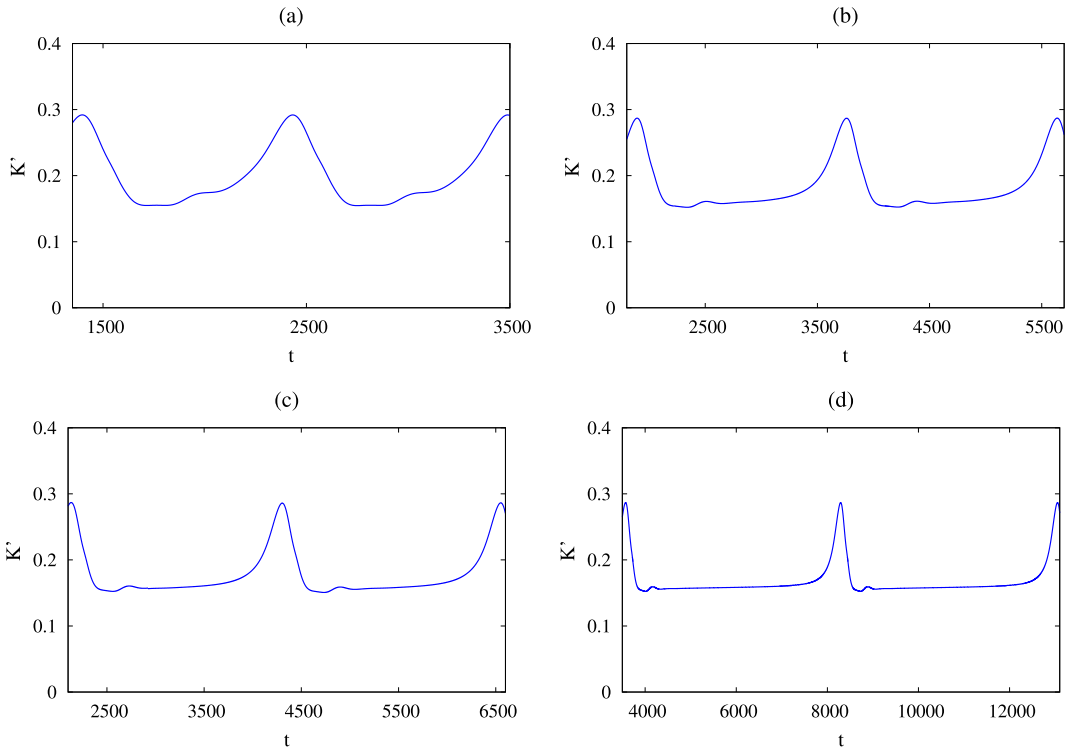

Fig. 1. Perturbation energy associated with the relative periodic orbit solutions computed with the edge-tracking procedure for the selected increasing values of the spanwise size $L_z = 3.525$, $L_z = 3.535$, $L_z = 3.540$, $L_z = 3.548$ (panels (a) to (d)). The initial transient before the convergence to the edge state is discarded. Remark the increasing period of the solutions as L_z is increased.

3. Results

3.1. From relative periodic orbits to travelling waves

In a previous investigation [15], relative periodic solutions were computed in plane Poiseuille flow in the domain of extension $2\pi \times 2 \times 2.416$, for which Waleffe's travelling-wave solutions appear at the lowest Reynolds number [3], and for Reynolds numbers ranging from $Re = 2000$ to 5000. The period T of these solutions increased with the Reynolds number ($T = 368$ for $Re = 2000$, $T = 739$ for $Re = 3000$, $T = 1090$ for $Re = 4000$ and $T = 1418$ for $Re = 5000$) and the solutions were found to travel in the streamwise direction with a phase speed $C_x \approx 0.98$. We have not found it possible to continue these periodic solutions much below $Re = 2000$, leaving obscure their origin. Previous investigations of plane Couette flow, however, showed that the Nagata–Clever–Busse–Waleffe branch of steady solutions can be connected to a branch of periodic solutions by changing the size of the box [7]. We have therefore continued the relative periodic orbit solution obtained at $L_z = 2.416$ to higher values of L_z by using edge-tracking in the $\pm y$ symmetric subspace while keeping constant the Reynolds number to $Re = 2000$ and the streamwise box dimension to $L_x = 2\pi$.

When L_z is increased the periodic solutions display increasingly long quiescent phases separated by relatively quick bursts, as shown in Fig. 1. This leads to an increase in the period T of the solutions with L_z. For values above $L_z \approx 3.55$ the edge tracking converges to a travelling wave (TW) solution instead of a relative periodic orbit. The continuation of the TW solution in L_z using pseudo-arclength continuation based on the Newton-based iterations of `peanuts` reveals the existence of an upper and of a lower branch of solutions connected by a saddle node bifurcation at $L_z^* = 3.55$, as shown in Fig. 2(a) and in Fig. 3.

The bifurcation observed at L_z^* is global and is associated with a divergence of the period T of the periodic solutions while approaching the bifurcation. As shown in Fig. 2(b), the data are well matched by the fit $T = 240/\sqrt{\mu}$, where $\mu = (L_z^* - L_z)/L_z^*$. The divergence of T as $\mu^{-1/2}$ and the $O(1)$ amplitude of the periodic solution while approaching the critical value L_z^* are the hallmark of the saddle-node infinite-period bifurcation, where a periodic solution is replaced by a pair of fixed points (see, e.g., [27]). The same type of global bifurcation has already been found, e.g., in the study of axisymmetric convection [28] and, more recently, in the homotopy of plane Couette flow travelling-wave solutions that are continued to asymptotic suction boundary layer (ASBL) solutions by increasing the suction velocity on the lower wall [12]. In all these cases, including ours, an upper and a lower branch travelling-wave solutions and their spanwise shifted heteroclinically connected copy collide in phase space at L_z^*, in a pair of saddle-node bifurcations, which results in the formation of a periodic solution, which repeats itself with a shift symmetry every $T/2$.

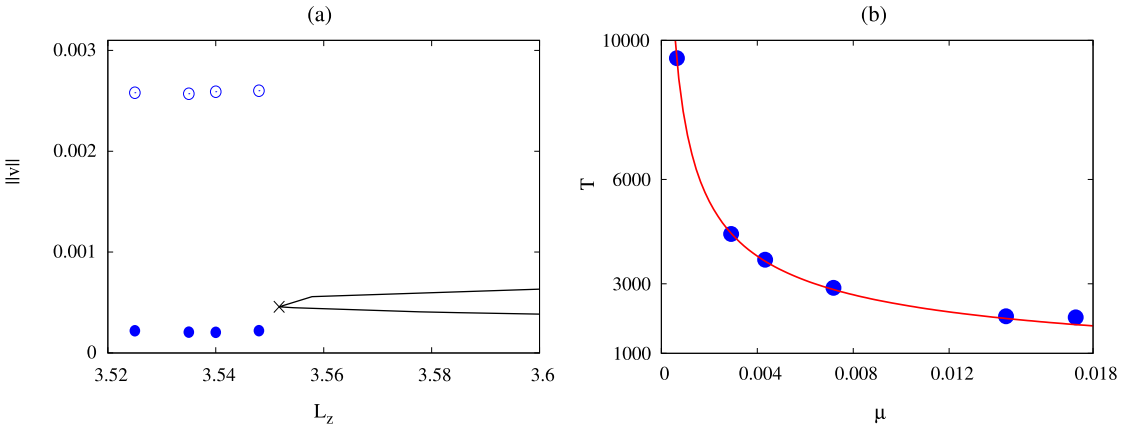

Fig. 2. (a) Bifurcation diagram in L_z, with $L_x = 2\pi$ and $Re = 2000$, where the relative periodic orbit solution disappears in a global saddle-node infinite-period bifurcation originating a pair of travelling-wave solutions. The periodic solution is reported with its maximum (empty symbols) and minimum (filled symbols) values of the spatially-averaged wall-normal velocity. The symbols correspond to the L_z values considered in Fig. 1. The point where the upper- and lower-branch travelling-wave solutions are generated is denoted by the X symbol. (b) Variation of time period T close to the bifurcation point. The function $T \approx 240/\sqrt{\mu}$ (solid line), where $\mu = (L_z^* - L_z)/L_z^*$, fits well the data (symbols). The four leftmost symbols correspond to the time-series reported in Fig. 1.

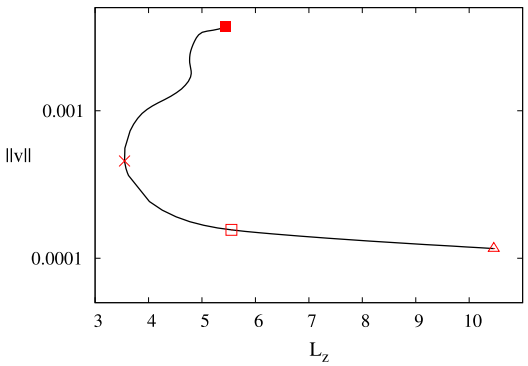

Fig. 3. Continuation diagram for travelling-wave solutions as a function of L_z, with $L_x = 2\pi$ and $Re = 2000$. The left-most part of the diagram is already reported in Fig. 2(a). The turning point where the upper and lower branch of the travelling-wave solution originate corresponds to the saddle-node infinite period global bifurcation.

3.2. Structure of travelling-wave solutions

The flow structures associated with the travelling-wave solution at the bifurcation consist of the usual sinuously bent low-speed streak flanked by a pair of quasi-streamwise vortices, as shown in Fig. 4(a). When this solution is continued to higher values of L_z along the lower branch, at least up to $L_z = 10.5$, the streaky structure remains unique and becomes localized in the spanwise direction, leaving an increasingly large portion of the domain almost unperturbed, as shown in Fig. 4(b) and (c)) These localized structures, which arise 'naturally' through continuation without the need to use a windowing function as, e.g., in [29], are unstable. For $L_z = 10.5$ the unique unstable eigenvalue found is 5.79×10^{-3} and is therefore an edge state as can be verified by perturbing the solution along its unstable manifold, i.e. with the unstable eigenfunction. It is indeed found that this perturbation leads to a turbulent state or to a fast decay to the laminar state depending on the sign of the perturbation, as shown in Fig. 5. The observed spanwise localization of the lower-branch solution is similar to that observed in a number of other flows [30–32,29], and therefore seems to be a generic property of lower-branch solutions in shear flows.

The evolution of the upper-branch travelling-wave solution is completely different. In this case, indeed, continuation to higher values of L_z leads to an increase in the number of streaky structures. For instance, at $L_z = 5.55$, as reported in Fig. 6(b), the upper-branch solution contains three low-speed streaks and three pairs of quasi-streamwise vortices, which correspond to a streak spacing $\lambda_z \approx 1.8$, in good agreement with the size of large-scale motions (LSM) in the turbulent channel [33,22]. This spacing is confirmed by the analysis of the spanwise premultiplied spectrum of the streamwise velocity (not shown). The energy of the upper-branch solutions increases for increasing L_z. In Fig. 7, it can be seen that during the continuation the *rms* ($x-z$ averaged) profiles of the three velocity components preserve a qualitatively similar shape, which is also similar to that of the relative periodic solutions existing before the global bifurcation and this despite the changing nature of the underlying solutions.

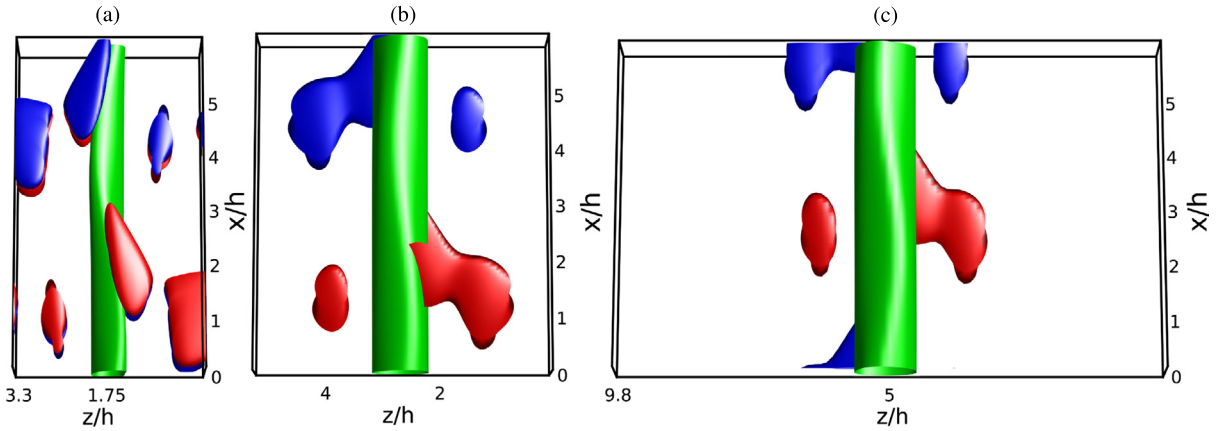

Fig. 4. Flow fields associated with the travelling-wave solutions corresponding to (a) the saddle node $L_z \approx 3.55$ ($\times$ symbol in Fig. 3), while (b) and (c) are the lower branch solution respectively computed for $L_z = 5.55$ (empty square symbol in Fig. 3) and $L_z = 10.5$ (empty triangle symbol in Fig. 3). The iso-surfaces at $u^+ = -2$ are plotted in green, while red and blue surfaces correspond to positive and negative streamwise vorticity at $\omega_x = \pm 0.65 \max(\omega_x)$.

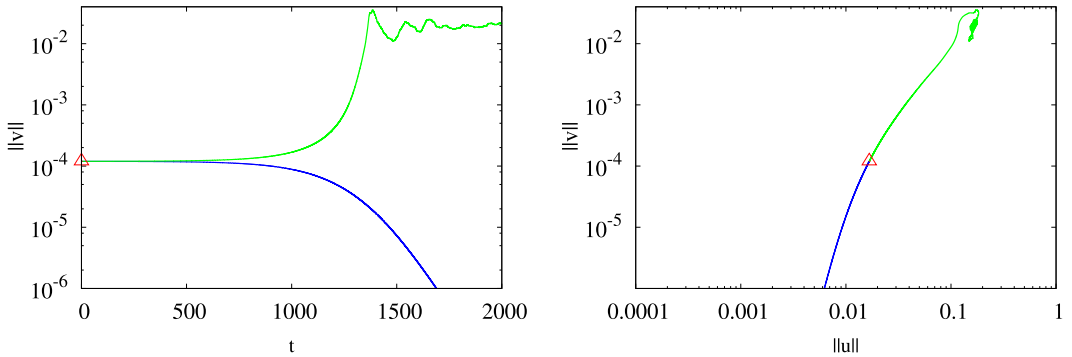

Fig. 5. Trajectories initialized along the unstable eigendirection of the lower branch spanwise localized travelling-wave solutions ($L_x = 2\pi$, $L_z = 10.5$, $Re = 2000$) and represented in the $t - \|u'\|$ (left panel) and $\|u'\| - \|v'\|$ (right panel) planes respectively. When initialized along one direction of the unstable manifold, the flow rapidly relaxes to the laminar Poiseuille solution (blue line). When initialized in the opposite direction, a turbulent state is attained (green line). This indicates that the lower branch localized state (red cross in the figure) sits on the edge of chaos.

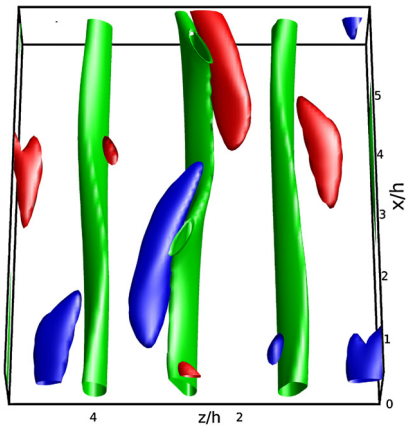

Fig. 6. Flow field associated with the upper branch solution computed at $L_z = 5.55$ corresponding to the filled square symbol in Fig. 3. The iso-surfaces at $u^+ = -2$ are plotted in green, while red and blue surfaces correspond to positive and negative streamwise vorticities at $\omega_x = \pm 0.65 \max(\omega_x)$.

Despite the changing nature of these solutions, it has been impossible to continue the upper branch to values larger than $L_z \approx 5.57$. The relevance of the upper-branch solution to the dynamics of turbulent large-scale coherent structures is further investigated using filtered large-eddy simulations to include the locally averaged effect of small-scale motions, as discussed in the next section.

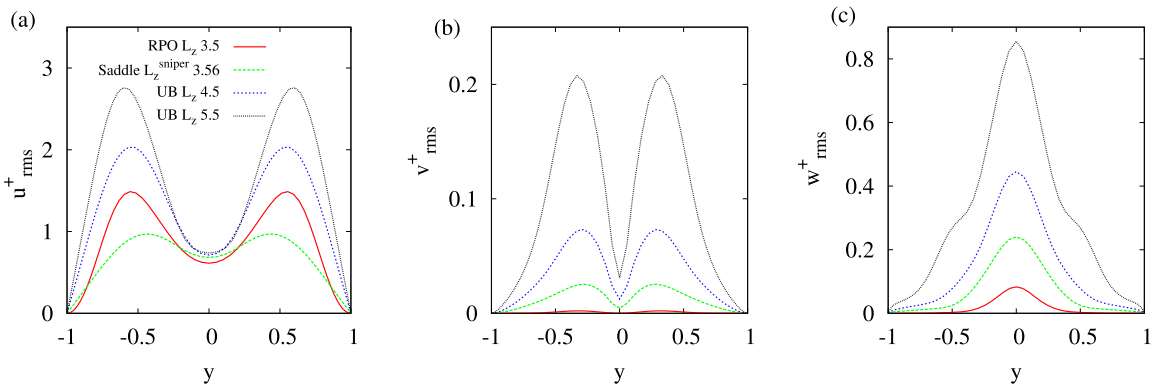

Fig. 7. Comparison of the *rms* velocity profiles of the travelling-wave upper branch solutions for selected values of L_z to the *rmr* profiles of the relative periodic orbit solutions existing for $L_z < L_z^*$.

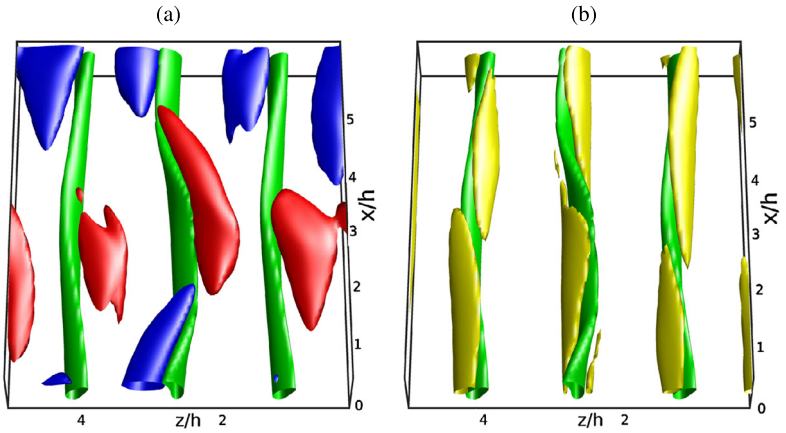

Fig. 8. Flow field associated with the upper branch solutions to the filtered (LES) equations computed at $L_z = 5.55$ for $C_s = 0.05$. The iso-surfaces at $u^+ = -2$ are plotted in green. In panel (a) red and blue surfaces correspond to positive and negative streamwise vorticity at $\omega_x = \pm 0.65 \max(\omega_x)$, while in panel (b) the yellow surface corresponds to $\nu_t/\nu = 0.065$.

3.3. Continuation from Navier–Stokes solutions to coherent solutions of the filtered equations

In a recent investigation [14], it was shown that invariant solutions to the Navier–Stokes equations can be continued to invariant solutions to the equations for filtered turbulent motions used in large-eddy simulations. In the equations used in large eddy simulations, small-scale motions are averaged by filtering and modelled by a sub-grid model. In [14] Smagorinky's 1963 model [21] was used along the lines of previous investigations of the self-sustained processes at large scale in turbulent shear flows [22,18]. In this context, the Smagorinsky constant C_s is used as a continuation parameter. The value $C_s = 0.05$ corresponds to large eddy simulations having good a posteriori agreement with direct numerical simulations [23], while Navier–Stokes solutions are obtained with $C_s = 0$.

We have therefore continued the travelling-wave upper branch solution from $C_s = 0$ (Navier–Stokes solution) to $C_s = 0.05$, keeping constant the Reynolds number to $Re = 2000$ and the grid. This corresponds to taking into account the locally averaged effect of dissipative small scale turbulent motions. Proceeding along these lines makes sense because $Re = 2000$ is more than twice the value of the Reynolds number at which transition is usually observed. The continuation proceeds without major problems and convergence is obtained in less than ten steps in C_s. It is found that the introduction of small-scale dissipation does not significantly alter the solutions, except for a slight reduction of the streamwise vorticity and of the streamwise velocity, and for the appearance of the sub-grid eddy viscosity shown in Figs. 8 and 9. The computed upper-branch travelling-wave solutions therefore can also be connected to large-scale coherent structures in a fully developed flow. To our knowledge, these solutions are the first coherent invariant solutions to the filtered (LES) equations computed for a plane pressure-driven channel.

4. Discussion and conclusions

This study has considered invariant solutions in plane Poiseuille flow. The main results can be summarized as follows:

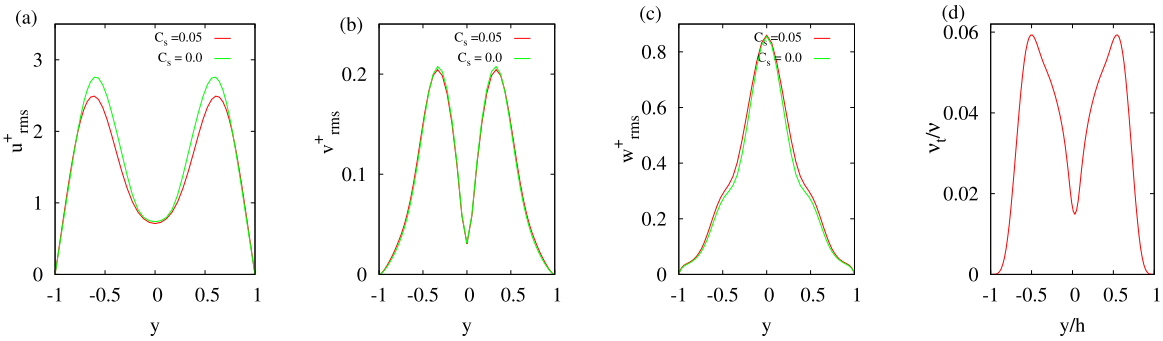

Fig. 9. Comparison of the *rms* velocity profiles of the TW upper branch solutions for $C_s = 0$ and $C_s = 0.05$ (with $L_z = 5.55$ and $Re = 2000$). In panel (d) is displayed the eddy viscosity ν_t/ν associated with the subgrid motions modelled in the solution to the filtered (LES) equations at $C_s = 0.05$.

- the relative periodic orbit solutions to the Navier–Stokes equations described in Ref. [15] are connected to two branches of travelling-wave solutions via a global saddle-node-infinite-period bifurcation when they are continued by increasing the spanwise size L_z of the numerical domain at $Re = 2000$,
- lower-branch travelling-wave solutions remain spanwise localized when L_z is further increased,
- upper-branch travelling-wave solutions develop multiple streaks when L_z is further increased,
- upper-branch solutions are not qualitatively changed when continued from Navier–Stokes solutions into coherent solutions to the filtered equations (used in large-eddy simulations) by increasing the Smagorinsky constant from $C_s = 0$ to $C_s = 0.05$ as in [14]. In the latter case, these solutions represent turbulent coherent large-scale motions associated with small-scale turbulent dissipation.

Many of these results suggest the existence of some kind of generic dynamics of invariant solutions in wall bounded flows. For instance, the dynamics of the relative periodic orbits from where our continuations start (see also [15]) is similar to that of relative periodic orbit solutions in the asymptotic boundary layer [12] in their $T/2 - L_z/2$ shift property and with their bursting behaviour. Also, the saddle-node infinite-period bifurcation found by increasing L_z is of the same type as that found in axi-symmetric Rayleigh–Bénard convection [28] or in the bifurcation found by homotopy continuation from Couette's flow to the asymptotic suction boundary layer by [12]. The spanwise localization of the lower-branch solution is also in accordance with the results of recent investigations, which revealed the spanwise localization of other lower-branch solutions [34,31,32,29].

One of the most relevant results shown in this study, however, is probably that the upper branch travelling-wave solutions are seen to develop multiple streaks in the spanwise direction when L_z is increased and that these solutions preserve their structure in the presence of small-scale dissipation. The wall-normal structure of the upper branch travelling-wave solutions, just as the one of the relative periodic orbits from which they are issued, is reminiscent of large-scale motions in the outer region, even if further work is needed to asses the dynamic relevance of these solutions. Further investigations are needed to determine if other travelling-wave or relative periodic-orbit solutions can be continued to the fully turbulent regime.

Acknowledgements

The use of the codes `channelflow` [25,35], `diablo` code [26] as well as financial support (grant n. 11050707) from PRES Université de Toulouse and Région Midi-Pyrénées are kindly acknowledged.

References

[1] M. Nagata, Three-dimensional finite-amplitude solutions in plane Couette flow: bifurcation from infinity, J. Fluid Mech. 217 (1990) 519–527.
[2] U. Ehrenstein, W. Koch, Three-dimensional wavelike equilibrium states in plane Poiseuille flow, J. Fluid Mech. 228 (1991) 111–148.
[3] F. Waleffe, Homotopy of exact coherent structures in plane shear flows, Phys. Fluids 15 (2003) 1517–1534.
[4] H. Faisst, B. Eckhardt, Travelling waves in pipe flow, Phys. Rev. Lett. 91 (2003) 224502.
[5] H. Wedin, R.R. Kerswell, Exact coherent structures in pipe flow: travelling wave solutions, J. Fluid Mech. 508 (2004) 333–371.
[6] R.M. Clever, F.H. Busse, Tertiary and quaternary solutions for plane Couette flow, J. Fluid Mech. 344 (1997) 137–153.
[7] G. Kawahara, S. Kida, Periodic motion embedded in plane Couette turbulence: regeneration cycle and burst, J. Fluid Mech. 449 (2001) 291–300.
[8] D. Viswanath, The dynamics of transition to turbulence in plane Couette flow, physics/0701337, 2007.
[9] S. Toh, T. Itano, A periodic-like solution in channel flow, J. Fluid Mech. 481 (2003) 67–76.
[10] Y. Duguet, C.C.T. Pringle, R.R. Kerswell, Relative periodic orbits in transitional pipe flow, Phys. Fluids 20 (11) (2008) 114102.
[11] T. Kreilos, B. Eckhardt, Periodic orbits near onset of chaos in plane Couette flow, Chaos 22 (4) (2012) 047505.
[12] T. Kreilos, G. Veble, T.M. Schneider, B. Eckhardt, Edge states for the turbulence transition in the asymptotic suction boundary layer, J. Fluid Mech. 726 (2013) 100–122.
[13] A. Riols, F. Rincon, C. Cossu, G. Lesur, P.-Y. Longaretti, G.I. Ogilvie, J. Herault, Global bifurcations to subcritical magnetorotational dynamo action in Keplerian shear flow, J. Fluid Mech. 731 (2013) 1–45.

[14] S. Rawat, C. Cossu, Y. Hwang, F. Rincon, On the self-sustained nature of large-scale motions in turbulent Couette flow, J. Fluid Mech. 782 (2015) 515–540.
[15] S. Rawat, C. Cossu, F. Rincon, Relative periodic orbits in plane Poiseuille flow, C. R. Mecanique 342 (2014) 485–489.
[16] T. Itano, S. Toh, The dynamics of bursting process in wall turbulence, J. Phys. Soc. Jpn. 70 (2001) 703–716.
[17] Y. Hwang, C. Cossu, Linear non-normal energy amplification of harmonic and stochastic forcing in turbulent channel flow, J. Fluid Mech. 664 (2010) 51–73.
[18] Y. Hwang, C. Cossu, Self-sustained processes in the logarithmic layer of turbulent channel flows, Phys. Fluids 23 (2011) 061702.
[19] P.E. Deardorff, A numerical study of three-dimensional turbulent channel flow at large Reynolds numbers, J. Fluid Mech. 41 (1970) 453–480.
[20] P. Sagaut, Large Eddy Simulation for Incompressible Flows: An Introduction, Springer Verlag, 2006.
[21] J. Smagorinsky, General circulation experiments with the primitive equations, I: the basic equations, Mon. Weather Rev. 91 (1963) 99–164.
[22] Y. Hwang, C. Cossu, Self-sustained process at large scales in turbulent channel flow, Phys. Rev. Lett. 105 (4) (2010) 044505.
[23] C. Härtel, L. Kleiser, Analysis and modelling of subgrid-scale motions in near-wall turbulence, J. Fluid Mech 356 (1998) 327–352.
[24] J. Herault, F. Rincon, C. Cossu, G. Lesur, G.I. Ogilvie, P.Y. Longaretti, Periodic magnetorotational dynamo action as a prototype of nonlinear magnetic field generation in shear flows, Phys. Rev. E 84 (2011) 036321.
[25] J.F. Gibson, J. Halcrow, P. Cvitanovic, Visualizing the geometry of state space in plane Couette flow, J. Fluid Mech. 611 (2008) 107–130.
[26] T.R. Bewley, Numerical Renaissance: Simulation, Optimization and Control, Renaissance Press, San Diego, CA, USA, 2008.
[27] S. Strogatz, Nonlinear Dynamics and Chaos: With Applications to Physics, Biology, Chemistry and Engineering, Perseus Books Group, 2001.
[28] L.S. Tuckerman, D. Barkley, Global bifurcation to travelling waves in axisymmetric convection, Phys. Rev. Lett. 61 (1988) 408–411.
[29] J.F. Gibson, E. Brand, Spanwise-localized solutions of plane shear flows, J. Fluid Mech. 745 (2014) 25–61.
[30] Y. Duguet, P. Schlatter, D.S. Henningson, Localized edge states in plane Couette flow, Phys. Fluids 21 (11) (2009) 111701.
[31] Y. Duguet, P. Schlatter, D.S. Henningson, B. Eckhardt, Self-sustained localized structures in a boundary-layer flow, Phys. Rev. Lett. 108 (4) (2012) 044501.
[32] T. Khapko, T. Kreilos, P. Schlatter, Y. Duguet, B. Eckhardt, D.S. Henningson, Localized edge states in the asymptotic suction boundary layer, J. Fluid Mech. 717 (2013) R6.
[33] J.C. del Álamo, J. Jiménez, Spectra of the very large anisotropic scales in turbulent channels, Phys. Fluids 15 (2003) L41.
[34] T.M. Schneider, D. Marinc, B. Eckhardt, Localized edge states nucleate turbulence in extended plane Couette cells, J. Fluid Mech. 646 (2010) 441–451.
[35] J.F. Gibson, Channelflow: A Spectral Navier–Stokes Simulator in C++, Technical report, University of New Hampshire, Durham, NH, USA, 2012.